

# Modelling paradigms for MILD combustion

Y. Minamoto and N. Swaminathan\*

Department of Engineering, Cambridge University, Cambridge, CB2 1PZ, UK.

\*Corresponding author:

Department of Engineering, Cambridge University,  
Trumpington Street, Cambridge, CB2 1PZ, UK.

E-mail: ns341@cam.ac.uk.

Phone: +44(0)1223 332586.

Fax: +44(0)1223 339906.

(Date: October 25, 2013)

Running Title: Modelling of MILD combustion

Submitted to International Journal of Advances in Engineering Sciences and Applied Mathematics (Special Issue on Combustion)

## Abstract

Three-dimensional Direct Numerical Simulation (DNS) data of methane-air MILD combustion is analysed to study the behaviour of MILD reaction zones and to identify a suitable modelling paradigm for MILD combustion. The combustion kinetics in the DNS was modelled using a skeletal mechanism including non-unity Lewis number effects. The reaction zones under MILD conditions are highly convoluted and contorted resulting in their frequent interactions. This leads to combustion occurring over a large portion of the computational volume and giving an appearance of distributed combustion. Three paradigms, standard flamelets, mild flame elements (MIFEs) and PSR, along with a presumed PDF model are explored to estimate the mean and filtered reaction rate in MILD combustion. A beta function is used to estimate the presumed PDF shape. The variations of species mass fractions and reaction rate with temperature computed using these models are compared to the DNS results. The PSR-based model is found to be appropriate, since the conditional averages obtained from the DNS agree well with those obtained using the PSR model. The flamelets model with MIFEs gives only a qualitative agreement because it does not include the effects of reaction zone interactions.

*Keywords:* MILD combustion, Flameless combustion, Direct numerical simulation (DNS), Perfectly stirred reactor (PSR), presumed PDF, LES, RANS, Modelling

# 1 Introduction

Moderate or Intense Low-oxygen Dilution (MILD) combustion concept has potentials to improve combustion efficiency and reduce pollutants emission simultaneously (Wünning & Wünning, 1997; Katsuki & Hasegawa, 1998; Cavaliere & de Joannon, 2004). The standard definition of MILD combustion condition is that (1) the local reactant temperature  $T_r$  is higher than the autoignition temperature of a given fuel  $T_{ign}$  and (2) the temperature increase during combustion,  $\Delta T = T_p - T_r$ , is lower than the autoignition temperature. The product temperature  $T_p$  is very low compared to that in conventional combustion even with the elevated reactant temperature, because the reactant mixture is diluted with a large amount of exhaust gas, giving a typical oxygen mole fraction in the local reactant mixtures of about 2 to 5%, ie.,  $X_{O_2,r} = 0.02 - 0.05$  (Cavaliere & de Joannon, 2004). These unique conditions given above can be summarised in a combustion type diagram to be shown later in section 2.2, and these conditions are key for the following advantages of MILD combustion.

Firstly, the combustion efficiency is enhanced due to the recovery of exhaust heat which is used to preheated reactants. Secondly, the maximum flame temperature under MILD conditions is typically less than 1900 K (Wünning & Wünning, 1997; Cavaliere & de Joannon, 2004). This low flame temperature together with low oxygen concentration resulting from dilution helps to reduce thermal NO formation. Thirdly, a combustion condition of large  $T_r$  and small  $\Delta T$  helps to suppress combustion noise and instabilities which are caused especially when the exhaust gas recycling rate, defined as the mass ratio between exhaust gas to fresh reactants, exceeds 30% for normal ambient air (Wünning & Wünning, 1997; Katsuki & Hasegawa, 1998). Also combustion can be sustained in a high-velocity jet field without internal recirculation zones because of highly preheated mixture (Wünning & Wünning, 1997; Cavaliere & de Joannon, 2004; Medwell *et al.*, 2007). Thus, the design of MILD combustor is no longer constrained by the requirements

of recirculation zones or a flame holder. Furthermore, the diluted and preheated combustion conditions are achieved relatively in a straightforward manner in practical devices by using conventional techniques such as exhaust (EGR), flue gas recirculation (FGR) or staged fuel ignition (Wünnung & Wünnung, 1997; Cavaliere & de Joannon, 2004; Hayashi & Mizobuchi, 2011). Given these advantages, the MILD combustion technology might be useful as one of the “green” technologies for thermal power generation.

One distinctive feature of MILD combustion phenomena is that flames are not visible to the naked eyes (Wünnung & Wünnung, 1997). Direct photographs of MILD combustion obtained in the previous studies clearly show this (de Joannon *et al.*, 2000; Özdemir & Peters, 2001; Krishnamurthy *et al.*, 2009) and these observations were interpreted as distributed combustion without intense chemical activities or thin reaction zones. Temperature fields suggesting distributed combustion have been observed using laser thermometry in previous studies (Plessing *et al.*, 1998; Özdemir & Peters, 2001) although OH PLIF images reported in the same studies exhibit presence of thin reaction zones.

Modelling of MILD combustion has been carried out in the context of RANS (Reynolds Averaged Navier-Stokes) either by using an Eddy Dissipation Concept (EDC) model (Weber *et al.*, 2000; Orsino *et al.*, 2001; Christo & Dally, 2005; Galletti *et al.*, 2007; Aminian *et al.*, 2011; Parente *et al.*, 2011; Li & Mi, 2011) or a flamelet type model (Coelho & Peters, 2001; Dally *et al.*, 2004), and LES (Large Eddy Simulation) using a presumed subgrid probability density function (Duwig *et al.*, 2008; Ihme & See, 2012). In most RANS studies, the mean velocity and temperature fields show consistent trends with the experimental results. However, quantitative agreement of the calculated and measured temperature values becomes unsatisfactory as the dilution level increases (Christo & Dally, 2005). It is also reported that the prediction of minor species such as OH and CO is sensitive to the temperature fluctuation (Aminian *et al.*, 2011). Thus, predictions of temperature and mean reaction rate in MILD combustion are challenging. Past Direct Numerical Simulation (DNS) studies (Minamoto *et al.*, 2013; Minamoto & Swaminathan, 2013) showed

that the direct relation between a progress variable gradient and reaction rate observed for flamelets combustion is valid for the Reynolds averaged reaction rates in MILD combustion. However, these studies also showed that a conventional one-dimensional flamelet is not fully representative and a suitable model is yet to be developed to estimate the mean reaction rate in MILD combustion.

The main objective of this study is to propose a suitable model for MILD combustion. For this purpose, (1) the MILD reaction zone behaviour and its structure are investigated in detail using DNS data and (2) potential canonical models are explored and assessed using the DNS results for RANS and LES studies. These investigations are performed using the data obtained from three-dimensional DNS of methane-air MILD combustion. The DNS methodology, construction of initial mixture field, and combustion conditions are described briefly in the next section. The structure of MILD reaction zones is discussed in Section 3.4 after discussing general features of MILD combustion from the DNS results. Canonical models are proposed and assessed in Section 3.5. The conclusions are summarised in the final section.

## 2 DNS of MILD Combustion

The numerical code SENGA2 (Cant, 2012), an updated version of SENGA (Jenkins & Cant, 1999), is employed for this study. This code solves fully compressible governing equations for instantaneous mass, momentum, internal energy and scalar mass fractions on a uniform mesh, along with temperature dependent transport properties. The spatial derivatives are obtained using a tenth order central difference scheme which gradually reduces to a fourth order scheme near boundaries. The integration in time is achieved using a third order Runge-Kutta scheme. Methane-air combustion is simulated using a skeletal mechanism involving 16 species and 36 elementary reactions (Sooke & Giovangigli, 1991). The computational domain is cubic, having non-reflecting in- and out-flow bound-

aries (Poinsot & Lele, 1992) in the stream wise,  $x$ -direction, and periodic boundaries in the  $y$  and  $z$ -directions.

An inflowing mixture flows at an average velocity of  $U_{in}$  through the inflow boundary located at  $x = 0$  of the computational domain. On the inflow boundary, the scalar mass fractions,  $Y_i(x = 0, y, z, t)$ , temperature,  $T(x = 0, y, z, t)$ , and velocity,  $\mathbf{u}(x = 0, y, z, t)$ , are specified using preprocessed mixture fields  $\hat{Y}_i[\underline{x}(t), y, z]$ ,  $\hat{T}[\underline{x}(t), y, z]$  and  $\hat{\mathbf{u}}[\underline{x}(t), y, z]$ , where  $\underline{x}(t)$  denotes the  $x$  location of a scanning plane at time  $t$  moving at a velocity of  $U_{in}$  through the preprocessed fields. This inflowing mixture field is preprocessed as described in the next subsection, to mimic physical mixing and dilution process inherent for MILD mixtures. These computational steps are illustrated in Figure 1.

## 2.1 Flow configuration

The configurations such as EGR, flue gas recirculation (FGR) and staged fuel injection are used to achieve MILD combustion in practice by injecting fuel and air into a stream of hot products with a high momentum jet. It is unlikely that the mixtures are perfectly mixed before the reactions occur. In order to include these inhomogeneous mixture consisting of fresh and exhaust gases, the inflowing mixture field is constructed carefully taking the above physical processes into account through preprocessing steps. The details of these steps explained by Minamoto & Swaminathan (2013) are briefly summarised below.

First, a fully developed homogeneous isotropic turbulence field is obtained by conducting a DNS of freely decaying cold turbulence constructed using a specified initial spectrum (Rogallo, 1981). Second, an inhomogeneous progress variable field is obtained based on a scalar energy spectrum (Eswaran & Pope, 1987). Then, the mass fraction of species obtained from a one-dimensional freely propagating laminar flame, namely “Flame”, with desired MILD conditions are mapped on to the progress variable field. The initial temperature is set to a constant value of  $T_m$  to be specified later. These inhomogeneous species mass fraction and velocity fields are then allowed to evolve for about one

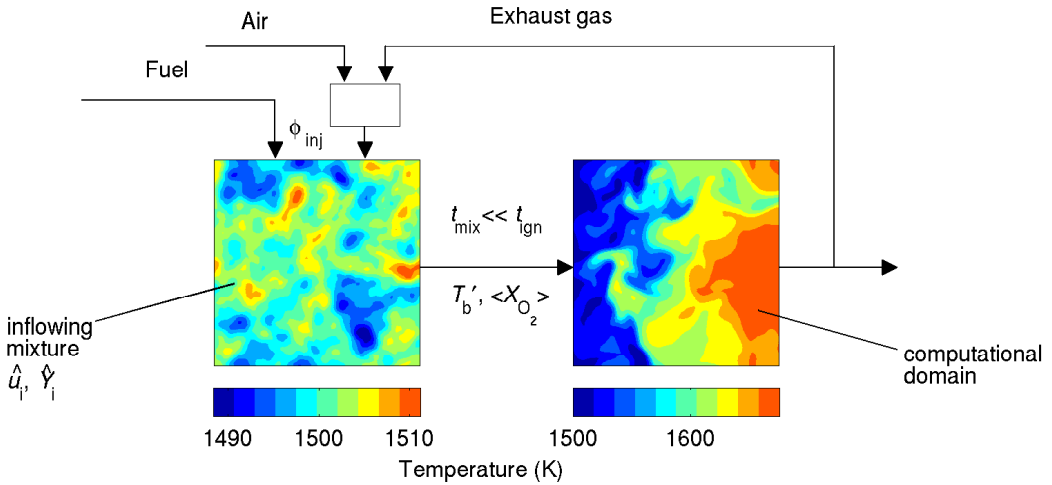


Figure 1. Schematic illustration of the DNS steps. Left box shows the preprocessed inflowing mixture field to be fed in a combustion DNS domain in the right.

large eddy turnover time in a periodic domain without any chemical reaction to mimic the EGR-mixing. This duration is sufficiently shorter than the autoignition delay time  $\tau_{ign}$  for the chosen mixture conditions to avoid autoignition. The internal energy equation is also solved during this mixing process, which creates a maximum temperature fluctuation of about 2% of the mean value,  $T_m$ . A sample temperature field in a mid  $x$ - $y$  plane at the end of the mixing DNS is shown on the left in Figure 1. The mean and variance of  $c_Y$  field at the end of the mixing DNS are respectively  $\langle c_Y \rangle \approx 0.50$  and  $\langle c_Y'^2 \rangle \approx 0.09$  for all MILD cases considered for this study. These preprocessed  $\hat{Y}_i$ ,  $\hat{T}$  and  $\hat{u}$  fields are used as the initial and inflowing mixture field for combustion DNS.

## 2.2 Turbulent combustion conditions

The velocity and scalar fields obtained as in Section 2.1 are used as initial and inflow fields for DNS of MILD combustion at atmospheric pressure. Two MILD cases are considered for this study. The mixture and turbulence conditions of these cases are given in Table 1, which are obtained from the preprocessed mixture field. Case A has a lower dilution than Case B, but the turbulence field used in the preprocessing steps are the same for

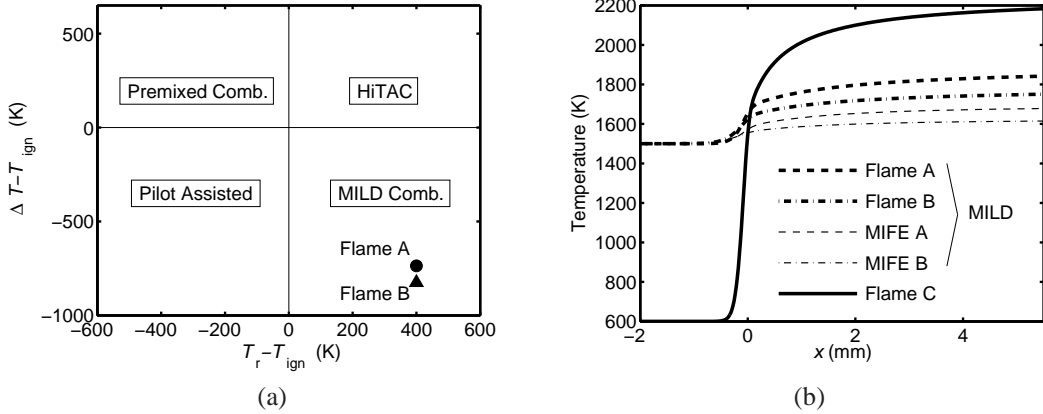


Figure 2. A diagram showing combustion types (Cavaliere & de Joannon, 2004) (a) and temperature variations in laminar MILD and conventional flames ( $x = 0$  is the peak location of the heat release rate) (b).

both cases resulting in almost the same turbulent fluctuations for these two cases. The difference in  $u'/S_L$  values given in Table 1 is because of the difference in  $S_L$  as one shall note later. The equivalence ratio is  $\phi = 0.8$  for both cases and the autoignition temperature of the given mixture is 1100 K. The inlet and initial mixture temperatures are set to be  $T_m \approx 1500$  K for the MILD combustion cases, which is comparable to that used in Suzukiwa *et al.* (1997). This inlet temperature and the intense dilution level used in this study (see Table 1) yield the combustion condition that is strictly in the MILD regime in the combustion type diagram shown in Figure 2a. Here, the conditions of the 1D laminar Flames A and B are shown, which are used in the initial/inlet field construction steps respectively for DNS of Cases A and B, as in Section 2.1.

The high dilution levels for the MILD combustion are indicated by the maximum,  $X_{O_2,r}^{\max}$ , and averaged,  $\langle X_{O_2,r} \rangle$ , mole fractions of oxygen in the reactant mixtures given in Table 1. The values of unstrained laminar flame speed,  $S_L$ , thermal thickness,  $\delta_{th} = (T_p - T_r)/|\nabla T|_{\max}$ , and the Zeldovich thickness,  $\delta_F = \alpha/S_L$ , are obtained based on appropriate planar unstrained laminar flames to be discussed in the next subsection. The mean,  $\langle \xi \rangle$ , and stoichiometric,  $\xi_{st}$ , mixture fraction values for the different cases are also given in Table 1. The normalised mean inflow velocity,  $U_{in}/S_L$ , is 9.6 for Case A and 15.1

Table 1. Combustion conditions of the 3D DNS.

	$X_{O_2,r}^{\max}$	$\langle X_{O_2,r} \rangle$	$\langle \xi \rangle$	$\xi_{st}$	$u'/S_L$	$l_0/\delta_F$	$l_0/\delta_{th}$	$Re_{l_0}$	Da	Ka
Case A	0.048	0.035	.011	.014	6.26	10.8	1.48	96.2	1.72	4.78
Case B	0.035	0.025	.008	.010	9.88	6.8	1.15	96.1	0.69	11.9

for Case B. Although the turbulence Reynolds number  $Re_{l_0}$  is relatively small, it is representative of typical values observed in experiments (Buschmann *et al.*, 1996; Chen *et al.*, 1996; Pfadler *et al.*, 2008) and in furnaces (Medwell *et al.*, 2007; Oldenhof *et al.*, 2011; Duwig *et al.*, 2012) with MILD combustion conditions. The Damköhler and Karlovitz numbers are calculated as  $Da = (l_0/\delta_F)/(u'/S_L)$  and  $Ka = (u'/S_L)^{3/2}(l_0/\delta_F)^{-1/2}$  respectively. Cases A and B are in the thin-reaction zones regime of the classical turbulent combustion regime diagram (Peters, 2000).

The computational domain has a dimension of  $L_x \times L_y \times L_z = 10.0 \times 10.0 \times 10.0 \text{ mm}^3$  for both cases. The domain is discretised using  $512 \times 512 \times 512$  mesh points for Case A and  $384 \times 384 \times 384$  mesh points for Case B. These meshes ensure that there are at least 30 mesh points inside the thermal thickness,  $\delta_{th}$ . The simulations were run for 1.5 flow-through times before collecting data for statistical analyses to ensure that the initial transients had left the domain. The flow-through time  $\tau_D$  is defined as the mean convection time,  $L_x/U_{in}$ , from the inflow to the outflow boundary. The simulations were then continued for one additional flow-through time and 80 data sets, including all the primitive variables, were collected.

### 2.2.1 MILD flame element

The Flames A and B, given in Table 2, are used in the construction of initial and inlet fields described in section 2.1 for MILD combustion Cases A and B respectively. However, the burnt side temperature for these laminar flames is much higher than that in the respective turbulent MILD cases. This is because the additional dilution effects due to the presence of exhaust gas pockets in the inflowing mixture field for the DNS is not taken

Table 2. Thermochemical conditions of 1D canonical laminar flames.

Flame	$X_{\text{CH}_4,r}$	$X_{\text{O}_2,r}$	$X_{\text{H}_2\text{O},r}$	$X_{\text{CO}_2,r}$	$T_r$ (K)	$T_p$ (K)	$S_L$ (m/s)	$\delta_F$ (mm)
Flame A	0.019	0.048	0.121	0.061	1500	1865	3.20	0.116
Flame B	0.014	0.035	0.132	0.066	1500	1775	2.15	0.168
Flame C	0.078	0.194	0.0	0.0	600	2179	1.18	0.064
MIFE A	0.0095	0.035	0.136	0.064	1500	1692	2.62	0.138
MIFE B	0.006	0.025	0.143	0.068	1500	1624	1.66	0.217

into account for the laminar flames. Thus, another canonical 1D laminar flame, named MILD Flame Element (MIFE), is proposed in this study. The reactant mixture of MIFE is constructed using volume averaged mass fractions of major species present in the inflowing mixture. Since the radicals and intermediates are excluded, the method of using the volume averaged mass fractions includes the dilution effects only partly. However, the burnt side temperatures for these laminar flames are close to those observed in the respective turbulent cases.

The thermochemical conditions of these laminar flames are summarised in Table 2. Here, a typical conventional laminar flame without dilution is also included as Flame C to compare with MILD cases. Figure 2b shows temperature variations with distance across these laminar flames. Despite their elevated reactant temperature Flames A and B have lower burnt side temperature than in Flame C because of dilution with products.

### 3 Results and Discussion

#### 3.1 Reaction rate and progress variable

The normalised reaction rate field  $\omega_{ct}^*$  is shown for both cases in Fig. 3. Here, the reaction rate is obtained as  $\omega_{ct} = Q/c_p(T_p - T_r)$ , where  $Q$  is the heat release rate and  $c_p$  is the specific heat capacity of the mixture. A superscript “+” in the rest of this paper denotes appropriately normalised value using  $\rho_r$ ,  $S_L$  and  $\delta_{th}$  obtained from the respective

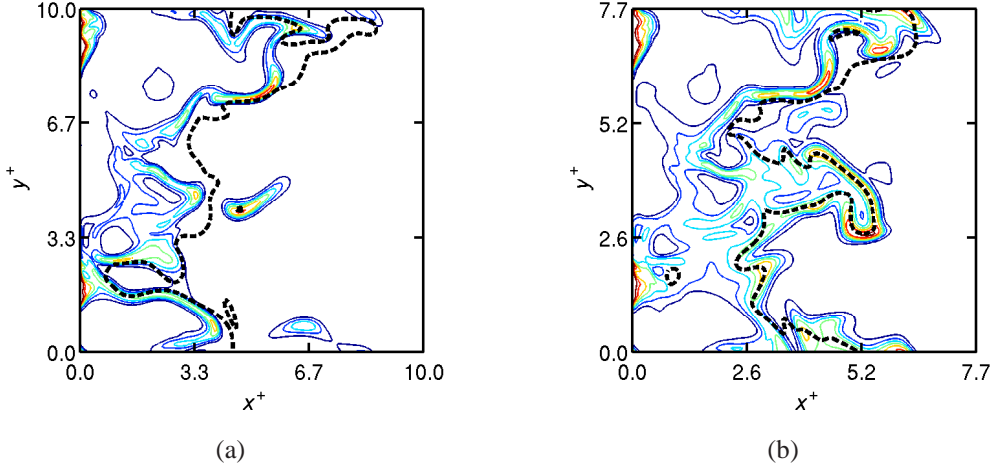


Figure 3. Contour of  $\omega_{cT}^* = 0.2, 0.3, \dots, 0.8$  (thin solid lines) in the mid  $x - y$  plane for (a) Case A and (b) Case B, where  $\omega_{cT}^*$  is the normalised reaction rate based on the global maximum value. A Contour for  $c_T = 0.6$  (thick dashed line) is also shown.

MIFE, where  $\rho_r$  is the reactant mixture density. For example, length and reaction rate are respectively normalised using  $\delta_{th}$  and  $\rho_r S_L / \delta_{th}$ .

The reaction zones of the MILD combustion cases shown in Figs. 3a and 3b are highly convoluted compared to the turbulent premixed flames having similar Da simulated in an earlier study (Trouv   & Poinsot, 1994). This suggests that the level of reaction zone convolution is not solely because of turbulence-chemistry interaction, but also because of the non-uniformity of an inflowing mixture field. The increased convolutions lead to interactions of reaction zones as shown in the figures. Such interactions eventually lead to distributed reaction zones as in Figure 3, which is also reported in a previous study (Minamoto *et al.*, 2013). The spatial extent of reaction zones (area with coloured contours in Fig. 3) is larger in Case B than Case A, due to increased dilution for Case B. Although thin reaction zones with a thickness of about  $\delta_{th}$  exist locally in both cases, distributed reaction zones having a thickness of almost 2 to 3  $\delta_{th}$  are observed in substantial part of the combustion domain. This observation suggests uniform combustion inside a volume of an average size of  $0.3\delta_{th}^3$ . This volume is typically made of pancake like structures for

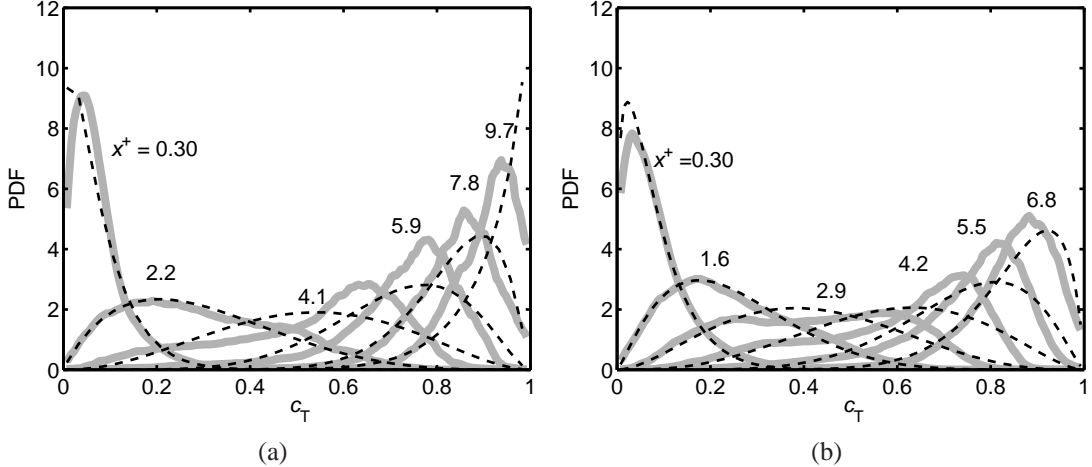


Figure 4. Probability density function of  $c_T$  (thick grey line) for Cases A (a) and B (b). The presumed PDF calculated using the  $\beta$ -function is also shown (thin dashed line).

the conditions of MILD combustion investigated in this study.

A contour of the reaction progress variable based on temperature,  $c_T = 0.6$ , is also shown in Fig. 3 using a dashed line. The reaction rate peaks at  $c_T \approx 0.6$  for the CH<sub>4</sub>-air premixed flames when a multi-step chemical kinetics is used (Swaminathan *et al.*, 2001) and this behaviour is not so strong in the MILD combustion cases shown in Fig. 3. The location of  $c_T = 0.6$  contour corresponds to intense reaction rate regions in some parts and weak reaction rate regions in other parts as shown in Fig. 3.

### 3.2 PDF of reaction progress variable

Figure 4 shows PDF of  $c_T$  for both cases. The data for the PDF is collected over the entire sampling period at particular  $x^+$  locations which are noted in the figure. The PDF shows distinct features unlike of standard turbulent premixed combustion in flamelets regime. At  $x^+ = 0.30$ , which is near the inlet boundary, the PDF has a relatively sharp peak at around  $c_T = 0.05$ , suggesting that cool gases are relatively predominant in this region. In the middle of the computational domain ( $x^+ = 2.2$  to  $5.9$  for Case A, and  $x^+ = 1.6$

to 4.2 for Case B), the PDF distribution is broad. As the sampling location goes further downstream, the probability of finding burnt gas becomes high. However, the bimodal behaviour is not observed, suggesting distributed combustion similar to those observed in previous experimental studies (Plessing *et al.*, 1998; Özdemir & Peters, 2001).

A comparison between Cases A and B shows that the maximum of PDF is generally larger in Case A than in Case B having a higher dilution. The laminar flame speed value,  $S_L$  is significantly reduced when the dilution level is increased resulting in a substantial change in Da for the same turbulence conditions as shown in Table 1. The results in Fig. 4 show that the PDF of  $c_T$  becomes more uniform without sharper peaks as the dilution level increases, which is suggestive of spatially uniform combustion with smaller scalar gradients compared to the classical turbulent premixed combustion.

The PDFs computed using the  $\beta$ -function model are also shown as dashed lines in Fig. 4. The  $\beta$ -function is based on the Favre mean  $\tilde{c}_T$  and variance  $\tilde{c}_T'^2$  of the progress variable calculated respectively as

$$\tilde{c}_T = \frac{\overline{\rho c_T}}{\overline{\rho}}, \quad \text{and} \quad \tilde{c}_T'^2 = \frac{\overline{\rho(c_T - \tilde{c}_T)^2}}{\overline{\rho}}. \quad (1)$$

Here, the Reynolds average, indicated by the over-bar, of a quantity  $Q$  is calculated as:

$$\overline{Q}(x) = \frac{1}{N_t N_y N_z} \sum_{n=1}^{N_t} \sum_{j=1}^{N_y} \sum_{k=1}^{N_z} Q(x; y_j, z_k, t_n), \quad (2)$$

where  $N_y$  and  $N_z$  are the number of mesh points in the  $y$  and  $z$ -directions respectively, and  $N_t$  is the number of data sets collected over the entire sampling period. Although there are small differences between the DNS and modelled PDFs, their shapes are well represented by the  $\beta$ -function model for both MILD cases.

Table 3. Thermochemical conditions for PSR models.

	$X_{\text{CH}_4}$	$X_{\text{O}_2}$	$X_{\text{H}_2\text{O}}$	$X_{\text{CO}_2}$	$T_r$ (K)	$T_p$ (K)	$\tau_{ign}$ (ms)
PSR A	0.0093	0.0345	0.135	0.064	1500	1667	0.285
PSR B	0.0059	0.0247	0.143	0.068	1500	1610	0.350

### 3.3 Modelling paradigms

In Sections 2.1 and 2.2, one-dimensional canonical laminar flames, called as Flames and MIFEs, are introduced for the present MILD combustion cases. However, as shown in Fig. 3, the reaction zones spread over a large part of the domain resulting in their interactions. Such reaction zones seem to have uniform combustion locally in a volume proportional to  $\delta_{th}^3$ . These attributes including the interacting flames may not be represented adequately by the models based on one-dimensional laminar flames.

Another possible modelling concept is to treat these reaction zones as perfectly stirred reactors (PSR) having representative residence time. A tabulated chemistry approach based on a PSR model has been used in a previous study (Duwig *et al.*, 2008). In the present study, the diluted reactant mixture composition for the PSR is based on volume averaged initial species mass fraction fields including radicals and intermediate species used for the DNS. Other initial parameters for the PSR are set based on the respective DNS conditions. The thermochemical conditions used for these PSR models are summarised in Table 3; PSR A is for DNS Case A, and PSR B is for Case B.

Based on the initial and inflowing conditions as in Table 3, the zero-dimensional unsteady PSR equations are solved for PSR A and PSR B using a commercial software COSILAB (2007). The simulation is continued until the reactor temperature reaches a nearly steady value which is close to the burnt temperature observed in the respective DNS. This PSR model is similar to the EDC approach (Magnussen, 1981; Ertesvag & Magnussen, 1996*a,b*) since it also assumes the local combustion zone to be a perfectly stirred reactor in the fine dissipative structure of turbulence having a volume of

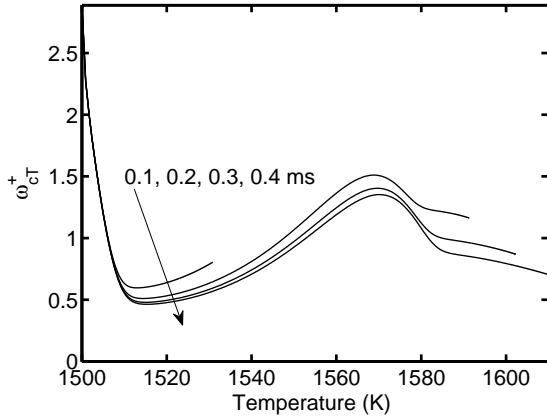


Figure 5. Reaction rate variation with temperature in an unsteady PSR for the mixture in Case B with various residence times ranging from 0.1 to 0.4 ms.

$V_{\text{EDC}}$  proportional to the cube of the Kolmogorov length scale,  $\eta$  (Magnussen, 1981; Ertesvag & Magnussen, 1996a,b). For the present modelling, the reactor volume is  $V_{\text{PSR}} \sim \delta_{th}^3$ . The ratio of these volumes is  $V_{\text{PSR}}/V_{\text{EDC}} \approx (\delta_{th}/\eta)^3 \approx \text{Ka}^{3/2}$  since  $\text{Ka} = (\delta_F/\eta)^2 \approx (\delta_{th}/\eta)^2$ . The values of Ka for the MILD cases considered in this study are greater than unity as given in Table 1 and thus the reactor volume is substantially larger than  $V_{\text{EDC}}$ . Thus, the residence time is set to be 0.4 ms which is similar to  $\tau_D$  for the DNS cases. It should be noted that this choice of the residence time allows one to get the complete variation of the reaction rate with  $c_T$  ranging from 0 to 1, which is obtained using the temperature at the exit of the PSR. The variation of the reaction rate with temperature at the PSR exit is shown in Fig. 5 for 4 different values of the residence time. Thus, local incomplete combustion can also be included in the estimate of mean or filtered reaction rate using this model.

### 3.4 Assessment of reaction zone structure

The variation of conditional average of species mass fraction,  $\langle Y_i | T \rangle$  with temperature, is shown in Fig. 6 for CH<sub>4</sub>, H<sub>2</sub>O, OH and CO for Cases A and B. This average is obtained using the DNS data from the entire sampling period. These results show that temper-

ature increases with consumption of  $\text{CH}_4$  and production of  $\text{H}_2\text{O}$ , and the radicals and intermediates exist over the entire temperature range shown in this figure. The variations obtained using the three models are also compared along with the DNS results. Among these models, Flames A and B yield poor agreements with the DNS results since they do not include dilution effects. This results in flame temperature being larger by about 150 K compared to the respective DNS value.

The results of MIFEs show good agreement with the respective DNS values for  $\langle Y_{\text{CH}_4}|T \rangle$  and  $\langle Y_{\text{H}_2\text{O}}|T \rangle$  as well as for other major species (not shown). The burnt mixture temperature for the MIFE is very close to the respective DNS value. This is because the dilution effects are included as explained in section 2.2. The maximum temperature for MIFEs differs by 27 K and 15 K respectively from the values observed in Cases A and B. The agreement between the DNS and MIFE values for  $\langle Y_{\text{OH}}|T \rangle$  is good up to around 1600 K for Cases A and B as shown in Fig. 6. However, the agreement becomes poor for  $T \geq 1600$  K, but the PSR model result is very good over the entire temperature range for all the species (see Fig. 6 for the variation of CO). Such a good agreement for the PSR model is because this model includes the dilution effects. Thus, the MILD combustion observed in the present cases is well represented by the paradigm involving the PSR model.

The variation of the conditional average of  $\langle \omega_Q|T \rangle$  is shown in Fig. 7 for Cases A and B, where  $\omega_Q = Q/c_p$ . The peak of  $\langle \omega_Q|T \rangle$  occurs at  $T \sim 1600$  K for Case A and 1550 K for Case B. The regions with peak  $\langle \omega_Q|T \rangle$  are close to  $c_T = 0.6$  contour shown in Fig. 3. The conditional reaction rate peaks at temperatures corresponding to about  $c_T = 0.6$  as shown in Fig. 7 and then drops with temperature because of the unavailability of  $\text{CH}_4$ . However, the conditional reaction rate does not reach zero due to the relatively slow post combustion reactions. One needs a very much larger computational domain than what is used in the current DNS to capture the drop of  $\omega_Q$  to zero.

The conditional average of  $\omega_Q$  is compared with those obtained using the three models

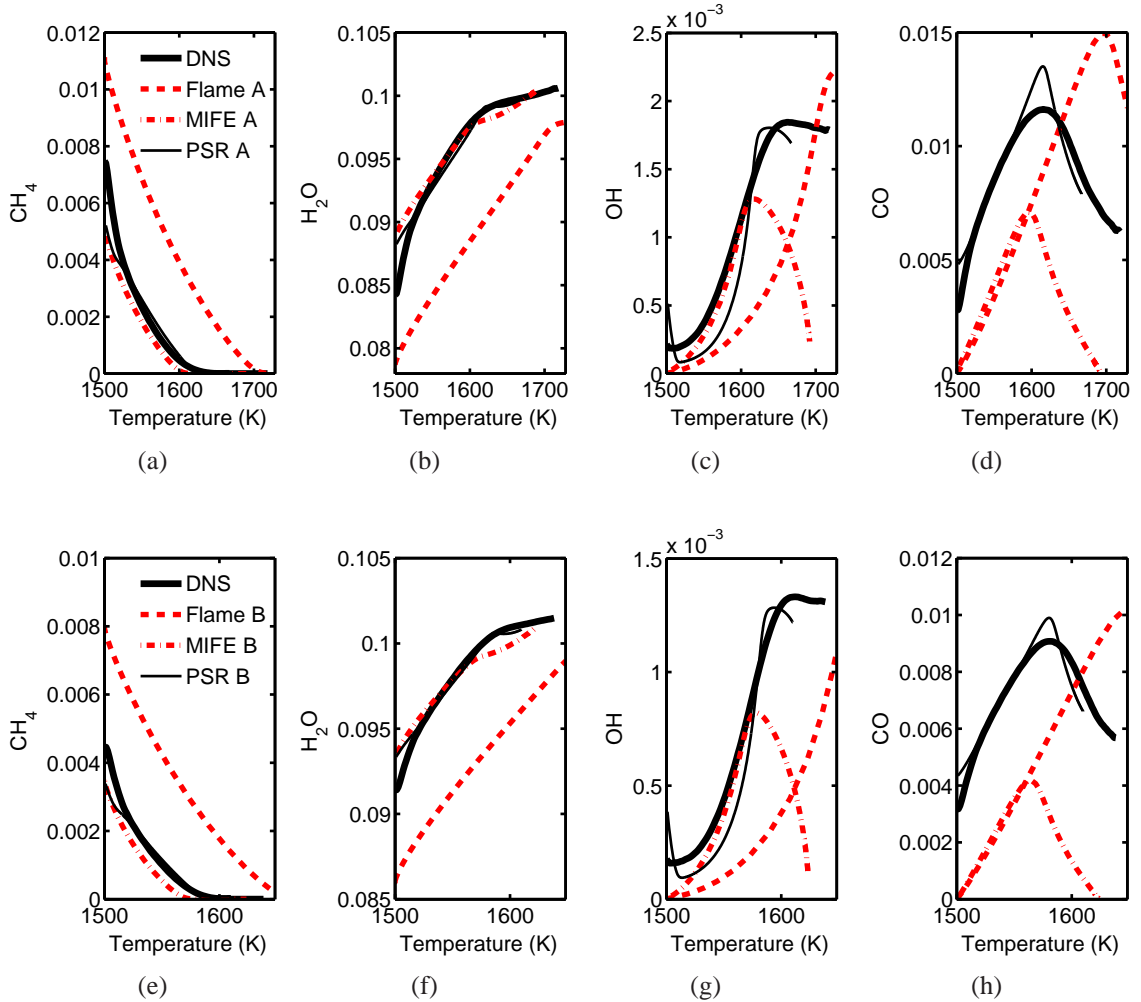


Figure 6. Variations of conditional mass fractions of  $\text{CH}_4$  (a, e),  $\text{H}_2\text{O}$  (b, f),  $\text{OH}$  (c, g), and  $\text{CO}$  (d, h) for Case A (a–d) and Case B (e–h) with temperature. Thick line: DNS result  $\langle Y_i | T \rangle$ , red dashed line: Flames A and B, red dash-dotted line: MIFEs A and B, and thin solid line: PSRs A and B.

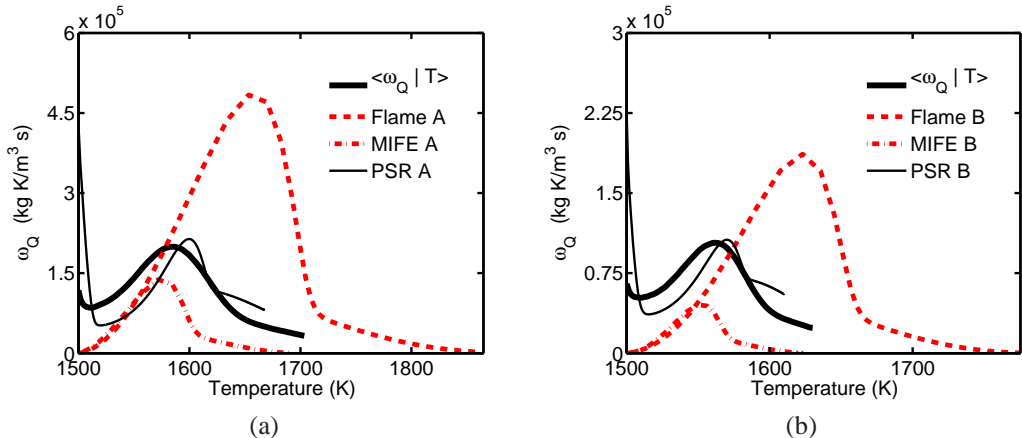


Figure 7. Variation of  $\omega_Q$  for (a) Case A and (b) Case B. Black thick line: DNS result  $\langle \omega_Q | T \rangle$ , red dashed line: Flames A and B, red dash-dotted line: MIFEs A and B, and thin solid line: PSRs A and B.

in Fig. 7. The reaction rate variations for the Flames A and B do not show good agreement with the respective DNS values. Although a qualitative agreement is seen for MIFE, it underestimates the reaction rate because the dilution effects are not included fully in the reactant mixture (the absence of radicals and intermediates as noted in section 2.2.1). Note that strained MIFEs are also considered; they do not yield adequate improvement than what is observed in Fig. 7 for the unstrained MIFEs and thus the results for strained MIFEs are not shown here. The PSR model shows a reasonable agreement with the respective DNS values of  $\langle \omega_Q | T \rangle$  although there is a small difference in the peak location. The conditionally averaged reaction rate for  $T = 1500$  K is significantly large for the PSR model and this arises from the nature of the inhomogeneous mixture used at the inlet boundary of the DNS domain. The radicals and intermediate species exist in a relatively smaller parts of this inhomogeneous mixture yielding smaller samples with large reaction rate for  $T = 1500$  K. This leads to a smaller conditionally averaged reaction rate for this temperature as shown in Fig. 7. For the PSR model, the mixture is homogeneous containing major, minor and intermediate species resulting in larger conditionally averaged reaction rate.

### 3.5 Assessment of averaged and filtered reaction rate

From the above discussion, it is clear that the MILD reaction zone structure is represented well by the PSR model. It has also been shown in section 3.2 that the  $\beta$  PDF is a reasonable model to represent the PDF of  $c_T$ . Thus, these two models can be combined together to estimate the mean reaction for RANS or filtered reaction rate for LES approaches. In the following discussion, this presumed PDF closure for the MILD combustion is assessed.

#### 3.5.1 Closure for averaged reaction rate

Using the presumed  $\beta$  PDF,  $P_\beta$ , the averaged reaction rate is written as

$$\bar{\omega}_{c_T} = \int_0^1 \omega(c_T) P_\beta(c_T) \, dc_T, \quad (3)$$

where  $\omega(c_T)$  is the reaction rate obtained from the MIFE or PSR model.

The variations of mean reaction rate in DNS with the streamwise distance  $x^+$  are shown in Fig. 8 for Cases A and B. Only MIFE and PSR models are assessed in this figure. The mean reaction rate obtained from the DNS results shows large values in the upstream region suggesting that the reactions occur as soon as the mixture enters the domain. Also, the mean reaction rate is non-zero over the entire computational domain. The MIFE model captures the DNS variation qualitatively and the modelled variations differ from the respective DNS result by about 2 to 3 times as shown in Fig. 8. The PSR model yields a good agreement with the respective DNS values as one would expect from the results discussed earlier. A similar level of agreement is also observed for the various species mass fractions for the PSR model. Thus, this RANS closure model is a good for MILD combustion, at least for the conditions considered in this study.

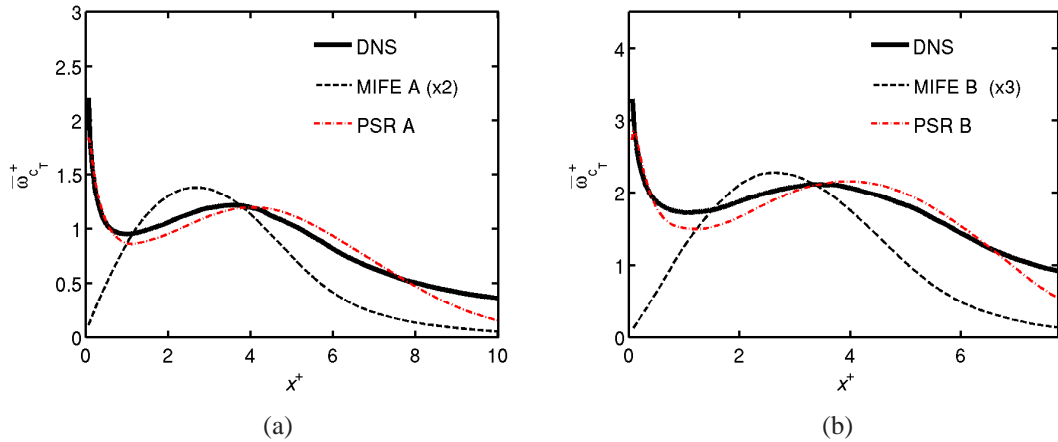


Figure 8. Comparison of mean and modelled reaction rates variation with  $x^+$  for (a) Case A and (b) Case B.

### 3.5.2 Closure for filtered reaction rate

The modelling approach in Eq. (3) can be extended to develop a closure for filtered reaction rate required in LES. This closure is written as

$$\langle \omega_{c_T} \rangle^{\text{model}}(\boldsymbol{x}, t) = \int_0^1 \omega(c_T) P_\beta(c_T; \boldsymbol{x}, t) \, dc_T, \quad (4)$$

where  $P_\beta$  is the subgrid PDF modelled using the  $\beta$ -function for a given value of filtered progress variable  $\langle c_T \rangle$  and subgrid variance  $\langle c_T''^2 \rangle$ . The angle brackets denote the filtered quantity. These values come from the solution of  $\langle c_T \rangle$  and  $\langle c_T''^2 \rangle$  transport equations in a LES calculation. For the model assessment conducted here, these values are obtained by post-processing the DNS results. The instantaneous reaction rate values in the DNS are filtered using a Gaussian filter having a filter width of  $\Delta = 3\delta_{th}$  for this analysis using

$$\langle \omega_{c_T} \rangle^{\text{DNS}}(\boldsymbol{x}, t) = \int \omega_{c_T}(\boldsymbol{x}', t) G(\boldsymbol{x} - \boldsymbol{x}'; \Delta) \, d\boldsymbol{x}', \quad (5)$$

where the filter kernel is given by

$$G(\mathbf{x} - \mathbf{x}'; \Delta) = \left( \frac{6}{\pi \Delta^2} \right)^{1/2} \exp \left( \frac{-6(\mathbf{x} - \mathbf{x}')^2}{\Delta^2} \right). \quad (6)$$

The modelled and filtered reaction rates, given by Eqs. (4) and (5) respectively, are unsteady field (3D) quantities. These quantities are averaged in the periodic directions for an easier comparison. This averaging is done, for example for the modelled values, using

$$\langle \omega_{c_T} \rangle^{\text{model}}(x, t) = \frac{1}{N_y N_z} \sum_{j=1}^{N_y} \sum_{k=1}^{N_z} \langle \omega_{c_T} \rangle^{\text{model}}(x, t; y_j, z_k). \quad (7)$$

A similar averaging is done for the instantaneous reaction rate to obtain  $\omega_{c_T}^{\text{DNS}}(x, t)$ . These averaged values, after normalised using  $\rho_r S_L / \delta_{th}$ , are compared in Fig. 9a for two different times,  $t = 1.5\tau_D$  and  $2.0\tau_D$ . This result is shown for Case B and it is similar for Case A. The variation of  $\omega_{c_T}^{+, \text{DNS}}(x, t)$ , filtered and modelled reaction rates are similar to that shown in Fig. 8. The filtered values,  $\langle \omega_{c_T}^+ \rangle^{\text{DNS}}(x, t)$ , represent the instantaneous reaction rates averaged in the periodic directions quite well and this variation of the filtered reaction rate is also captured quite well by the modelled values,  $\langle \omega_{c_T}^+ \rangle^{\text{model}}(x, t)$ , obtained using Eq. (7) for the PSR model. Since the comparison in Fig. 9a is shown for two instances and averaged in the periodic directions, a joint PDF of  $\langle \omega_{c_T}^+ \rangle^{\text{model}}$  and  $\langle \omega_{c_T}^+ \rangle^{\text{DNS}}$  for the samples collected over the entire sampling period is shown in Fig. 9b. If the agreement between the modelled and filtered reaction rates is uniformly good then the contours of joint PDF is expected to lie along the diagonal shown in Fig. 9b. Although there are small deviations suggesting some overestimate for large reaction rate, the agreement is reasonable and acceptable.

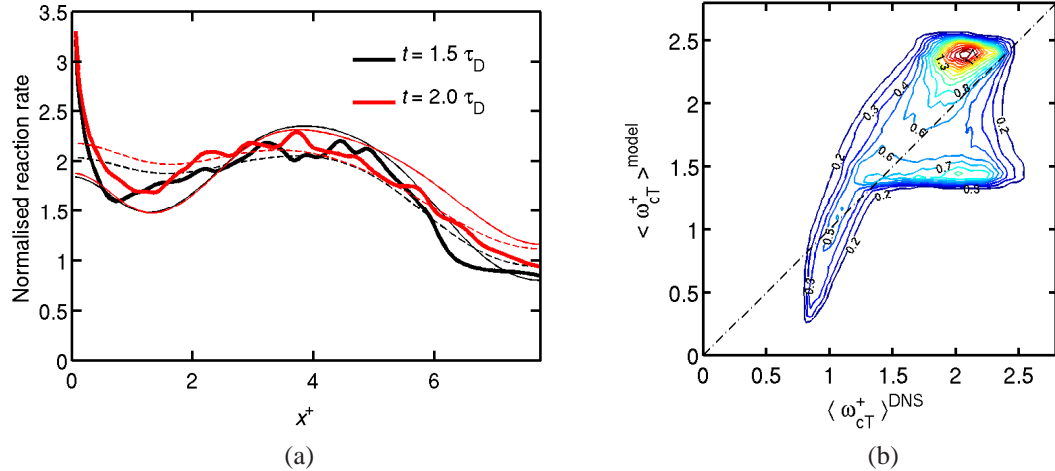


Figure 9. (a) Variation of  $\omega_{cT}^{+, \text{DNS}}(x, t)$  (thick solid lines),  $\langle \omega_{cT}^+ \rangle^{\text{DNS}}(x, t)$  (dashed lines)  $\langle \omega_{cT}^+ \rangle^{\text{model}}(x, t)$  (thin solid lines) with  $x^+$ . (b) Joint PDF of  $\langle \omega_{cT}^+ \rangle^{\text{DNS}}(x, t)$  and  $\langle \omega_{cT}^+ \rangle^{\text{model}}(x, t)$  from the samples collected over the entire sampling period. The PDF contours are for 0.2, 0.4,  $\dots$ , 1.8 values.

## 4 Summary and Conclusions

Direct numerical simulation data has been employed to identify and verify a suitable modelling paradigm for MILD combustion. The non-uniformity of diluted reactant mixture produces highly convoluted and contorted reaction zones resulting in frequent interactions. As a result of these interactions, MILD reaction zones spread over a large portion of the computational domain resulting in a relatively uniform combustion. This gives an appearance of distributed combustion under MILD conditions. Three different models, standard flamelets, MIFEs and PSRs, are explored to verify if the structure of the MILD reaction zones can be represented adequately to find a reasonable reaction rate closure for MILD combustion using presumed PDF approach. The performance of these models are verified using the DNS results. The standard flamelets, which do not include the dilution effects and flame interactions, seem to overestimate the species mass fraction and reaction rate variations with temperature. The strategy to include these effects in a flamelets approach is an open question at this time. Although both MIFEs and PSRs show potentials to represent reaction zones under MILD conditions, PSRs seem to be more suited because

of the bulk effects of dilution and reaction zones interaction resulting in uniform combustion over a volume proportional to  $\delta_{th}^3$  can be included effectively. The MIFEs and PSR models are applied in conjunction with presumed PDF approach to obtain a closure for the mean reaction rate required in RANS calculations of MILD combustion. This strategy is also extended to obtain a closure model for the filtered reaction rate required for LES calculations. The comparisons of these closure results to the DNS values suggests that the PSR model is very good for both RANS and LES methodologies.

## Acknowledgements

YM acknowledges the financial support of Nippon Keidanren and Cambridge Overseas Trust. EPSRC support is acknowledged by NS. This work made use of the facilities of HECToR, the UK's national high-performance computing service, which is provided by UoE HPCx Ltd at the University of Edinburgh, Cray Inc and NAG Ltd, and funded by the Office of Science and Technology through EPSRCs High End Computing Programme.

## References

- AMINIAN, J., GALLETTI, C., SHAHOSSEINI, S. & TOGNOTTI, L. 2011 Key modeling issues in prediction of minor species in diluted-preheated combustion conditions. *Appl. Thermal Eng.* **31**, 3287–3300.
- BUSCHMANN, A., DINKELACKER, F., SCHÄFER, T. & WOLFRUM, J. 1996 Measurement of the instantaneous detailed flame structure in turbulent premixed combustion. *Proc. Combust. Inst.* pp. 437–445.
- CANT, R. S. 2012 SENGA2 User Guide. In *Technical Report CUED/A-THERMO/TR67*. Cambridge University Engineering Department.

- CAVALIERE, A. & DE JOANNON, M. 2004 Mild combustion. *Prog. Energy Combust. Sci.* **30**, 329–366.
- CHEN, Y. C., PETERS, N., SCHNEEMANN, G. A., WRUCK, N., RENZ, U. & MANSOUR, M. S. 1996 The detailed flame structure of highly stretched turbulent premixed methane-air flames. *Combust. Flame* **107**, 223–244.
- CHRISTO, F. C. & DALLY, B. B. 2005 Modelling turbulent reacting jets issuing into a hot and diluted coflow. *Combust. Flame* **142**, 117–129.
- COELHO, P. J. & PETERS, N. 2001 Numerical simulation of a Mild combustion burner. *Combust. Flame* **124**, 503–518.
- COSILAB 2007 The Combustion Simulation Laboratory Version 2.0.8. Rotexo-Softpredict-Cosilab GmbH & Co. KG, Germany.
- DALLY, B. B., RIESMEIER, E. & PETERS, N. 2004 Effect of fuel mixture on moderate and intense low oxygen dilution combustion. *Combust. Flame* **137**, 418–431.
- DUWIG, C., LI, B. & ALDÉN, M. 2012 High resolution imaging of flameless and distributed turbulent combustion. *Combust. Flame* **159**, 306–316.
- DUWIG, C., STANKOVIC, D., FUCHS, L., LI, G. & GUTMARK, E. 2008 Experimental and numerical study of flameless combustion in a model gas turbine combustor. *Comb. Sci. Technol.* **180** (2), 279–295.
- ERTESVAG, I. S. & MAGNUSEN, B. F. 1996a A numerical study of a bluff-body stabilized diffusion flame. part 1. influence of turbulence modeling and boundary conditions. *Combust. Sci. Technol.* **119** (1-6), 171–190.
- ERTESVAG, I. S. & MAGNUSEN, B. F. 1996b A numerical study of a bluff-body stabilized diffusion flame. part 2. influence of combustion modeling and finite-rate chemistry. *Combust. Sci. Technol.* **119** (1-6), 191–217.

- ESWARAN, V. & POPE, S. B. 1987 Direct numerical simulations of the turbulent mixing of a passive scalar. *Phys. Fluids* **31** (3), 506–520.
- GALLETTI, C., PARENTE, A. & TOGNOTTI, L. 2007 Numerical and experimental investigation of a mild combustion burner. *Combust. Flame* **151**, 649–664.
- HAYASHI, S. & MIZOBUCHI, Y. 2011 Utilization of hot burnt gas for better control of combustion and emissions. In *Turbulent premixed flames* (ed. N. Swaminathan & K. N. C. Bray), pp. 365–378. Cambridge, UK: Cambridge University Press.
- IHME, M. & SEE, Y. C. 2012 Les flamelet modeling of a three-stream mild combustor: Analysis of flame sensitivity to scalar inflow conditions. *Proc. Combust. Inst.* **33**, 1309–1317.
- JENKINS, K.W. & CANT, R.S. 1999 Dns of turbulent flame kernels. In *Proc. Second AFOSR Conf. on DNS and LES* (ed. Knight & Sakell), pp. 192–202. Rutgers University, Kluwer Academic Publishers.
- DE JOANNON, M., SAPONARO, A. & CAVALIERE, A. 2000 Zero-dimensional analysis of diluted oxidation of methane in rich conditions. *Proc. Combust. Inst.* **28**, 1639–1646.
- KATSUKI, M. & HASEGAWA, T. 1998 The science and technology of combustion in highly preheated air. *Proc. Combust. Inst.* pp. 3135–3146.
- KRISHNAMURTHY, N., PAUL, P. J. & BLASIAK, W. 2009 Studies on low-intensity oxy-fuel burner. *Proc. Combust. Inst.* **32**, 3139–3146.
- LI, P. & MI, J. 2011 Influence of inlet dilution of reactants on premixed combustion in a recuperative furnace. *Flow Turbulence Combust.* **33**, 10.1007/s10494-011-9348-x.
- MAGNUSEN, B. F. 1981 On the structure of turbulence and a generalized eddy dissipation concept for chemical reaction in turbulent flow. *19th American Institute of Aeronautics and Astronautics Aerospace Science Meeting* pp. 1–6.

- MEDWELL, P. R., KALT, P. A. M. & DALLY, B. B. 2007 Simultaneous imaging of OH, formaldehyde, and temperature of turbulent nonpremixed jet flames in a heated and diluted coflow. *Combust. Flame* **148**, 48–61.
- MINAMOTO, Y., DUNSTAN, T. D., SWAMINATHAN, N. & CANT, R. S. 2013 DNS of EGR-type turbulent flame in MILD condition. *Proc. Combust. Inst.* **34**, 3231–3238.
- MINAMOTO, Y. & SWAMINATHAN, N. 2013 Scalar gradient behaviour in MILD combustion. *Combust. Flame* <http://dx.doi.org/10.1016/j.combustflame.2013.10.005>.
- OLDENHOF, E., TUMMERS, M. J., VAN VEEN, E. H. & ROEKAERTS, D. J. E. M. 2011 Role of entrainment in the stabilisation of jet-in-hot-coflow flames. *Combust. Flame* **158**, 1553–1563.
- ORSINO, S., WEBBER, R. & BOLLETTINI, U. 2001 Numerical simulation of combustion of natural gas with high-temperature air. *Comb. Sci. Technol.* **170** (1), 1–34.
- ÖZDEMİR, İ. B. & PETERS, N. 2001 Characteristics of the reaction zone in a combustor operating at MILD combustion. *Exp. Fluids* **30**, 683–695.
- PARENTE, A., GALLETTI, C. & TOGNOTTI, L. 2011 A simplified approach for predicting NO formation in MILD combustion of CH<sub>4</sub> – H<sub>2</sub> mixtures. *Proc. Combust. Inst.* **33**, 3343–3350.
- PETERS, N. 2000 *Turbulent combustion*. Cambridge, UK: Cambridge University Press.
- PFADLER, S., LEIPERTZ, A. & DINKELACKER, F. 2008 Systematic experiments on turbulent premixed Bunsen flame including turbulent flux measurement. *Combust. Flame* **152**, 616–631.
- PLESSING, T., PETERS, N. & WÜNNING, J. G. 1998 Laseroptical investigation of highly preheated combustion with strong exhaust gas recirculation. *Proc. Combust. Inst.* pp. 3197–3204.

- POINSOT, T. & LELE, S. 1992 Boundary conditions for direct simulations of compressible viscous flows. *J. Comput. Phys.* **101**, 104–129.
- ROGALLO, R. S. 1981 Numerical experiments in homogeneous turbulence. *NASA TM* p. 81315.
- SMOOKE, M. D. & GIOVANGIGLI, V. 1991 Formulation of the premixed and non-premixed test problems. In *Reduced kinetic mechanisms and asymptotic approximations for methane-air flames*. (ed. M. D. Smooke), , vol. 384, pp. 1–28. New York: Springer Verlag.
- SUZUKAWA, Y., SUGIYAMA, S., HINO, Y., ISHIOKA, M. & MORI, I. 1997 Heat transfer improvement and NO<sub>x</sub> reduction by highly preheated air combustion. *Energy Convers. Mgmt* **38** (10-13), 1061–1071.
- SWAMINATHAN, N., BILGER, R. W. & CUENOT, B. 2001 Relationship between turbulent scalar flux and conditional dilatation in premixed flames with complex chemistry. *Combust. Flame* **126**, 1764–1779.
- TROUVÉ, A. & POINSOT, T. 1994 The evolution equation for the flame surface density in turbulent premixed combustion. *J. Fluid Mech.* **278**, 1–31.
- WEBER, R., ORSINO, S., LALLEMAND, N. & VERLAAN, A. 2000 Combustion of natural gas with high-temperature air and large quantities of flue gas. *Proc. Combust. Inst.* **28**, 1315–1321.
- WÜNNING, J. A. & WÜNNING, J. G. 1997 Flameless oxidation to reduce thermal NO<sub>x</sub> formation. *Prog. Energy Combust. Sci.* **23**, 81–94.